



Power Electronic Systems  
Laboratory

© 2017 IEEE

Proceedings of the 8th International Symposium on Power Electronics for Distributed Generation Systems (PEDG 2017), Florianopolis, Brazil, April 17-20, 2017

## **10kV SiC-Based Bidirectional Soft-Switching Single-Phase AC/DC Converter Concept for Medium-Voltage Solid-State Transformers**

D. Rothmund,  
D. Bortis,  
J. Huber,  
D. Biadene,  
J. W. Kolar

This material is published in order to provide access to research results of the Power Electronic Systems Laboratory / D-ITET / ETH Zurich. Internal or personal use of this material is permitted. However, permission to reprint/republish this material for advertising or promotional purposes or for creating new collective works for resale or redistribution must be obtained from the copyright holder. By choosing to view this document, you agree to all provisions of the copyright laws protecting it.



Eidgenössische Technische Hochschule Zürich  
Swiss Federal Institute of Technology Zurich

# 10 kV SiC-Based Bidirectional Soft-Switching Single-Phase AC/DC Converter Concept for Medium-Voltage Solid-State Transformers

Daniel Rothmund\*, Dominik Bortis\*, Jonas Huber\*, Davide Biadene<sup>†‡</sup> and Johann W. Kolar\*

\* Power Electronic Systems Laboratory, ETH Zurich  
Email: rothmund@lem.ee.ethz.ch

<sup>†</sup> Dept. of Information Engineering, University of Padova  
<sup>‡</sup> Interdepartmental Centre G. Levi Cases

**Abstract**—State-of-the-art PWM AC/DC converters often suffer from high switching losses due to hard-switching and thus are limited in their efficiency and power density. In this paper, the concept of the *integrated* Triangular Current Mode (*i*TCM) operation is introduced, which enables soft-switching over the entire AC mains period and can overcome the limitation of PWM, resulting in a higher system performance. Thereby, an LC-circuit is added to the well-known full-bridge-based PWM AC/DC converter, which internally superimposes a high triangular current to the AC mains current in order to reverse the current direction in the semiconductors in each switching cycle and by this enabling soft-switching operation of all devices. In this paper, the *i*TCM concept is presented in detail and its performance is compared to the standard PWM and TCM approaches. Furthermore, the proposed *i*TCM concept is applied to a 10 kV SiC-MOSFET-based bidirectional 25 kW single-phase AC/DC converter operated from the 6.6 kV medium-voltage AC grid. In this case, compared to PWM, the *i*TCM concept allows to increase the switching frequency by almost a factor of five while the total semiconductor losses are reduced by more than 40 %.

## I. INTRODUCTION

Due to the ongoing trend towards higher energy efficiencies and power densities and the increasing number of grid-connected DC-loads and sources which range from high-power applications (e.g. photovoltaic power plants and battery charging facilities) down to low-power applications (e.g. PFC rectifiers in computer power supplies and consumer electronics), a high AC/DC conversion performance becomes more and more important. Most commonly, these rectifier/inverter stages are hard-switched PWM converters which typically suffer from comparably high switching losses, even if Wide Band Gap (WBG) semiconductors are employed, especially in case of high blocking voltage devices [1]–[4]. Consequently, the achievable efficiency and also the power density are strongly restricted, since the switching losses define an upper limit for the switching frequency, and hence inhibit a possible downsizing of passive components. The most effective strategy to reduce the switching losses is to apply soft-switching techniques and to profit from the typically much lower soft-switching losses compared to hard-switching.

Soft-switching can be achieved e.g. with the Triangular Current Mode (TCM) concept [5]–[8], where the boost inductance value is selected rather small in order to excite a

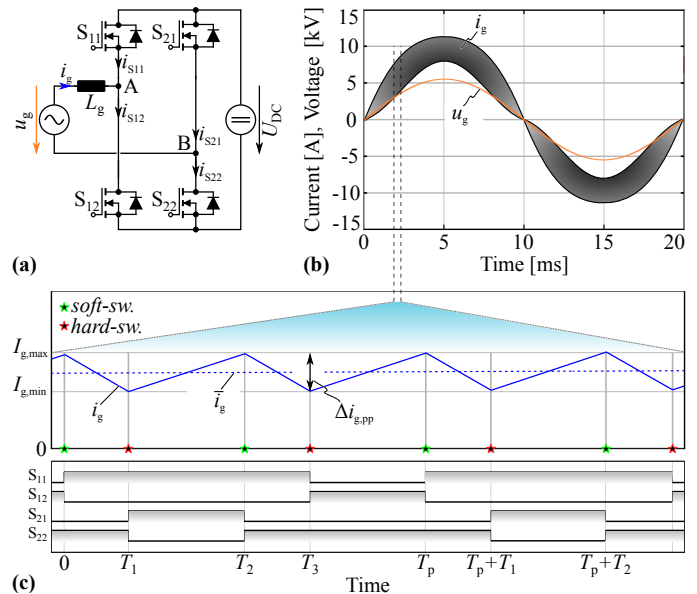


**Fig. 1:** (a) Circuit diagram of a bidirectional single-phase full-bridge AC/DC converter. (b) Waveforms of the grid voltage  $u_g$  and the grid current  $i_g$  over one grid period. (c) Detailed view of the grid current and the corresponding hard- and soft-switching transitions. The switching patterns of the two bridge-legs are phase-shifted by 180° in order to obtain unipolar PWM and a doubling of the effective switching frequency.

large high-frequency (HF) triangular current ripple in the boost inductor. The superposition of this HF triangular current to the instantaneous low-frequency (LF) grid current leads to a reversal of the current direction in the semiconductors and accordingly enables zero-voltage switching (ZVS) in each switching transition resulting in reduced semiconductor losses. On the other hand, however, with the TCM operation the boost inductor design becomes more challenging since both, the HF and the LF current, are flowing through the same inductor. In order to keep the HF losses in the inductor low, the employment of HF litz wire with thin strand diameter and HF core materials (e.g. ferrite) is necessary. Unfortunately, litz wire features a low copper filling factor and also the saturation flux density of HF core materials is typically low. However, in order to keep also the LF losses low, a winding with a high copper filling factor (i.e. solid copper wire) and a core material with a high saturation flux density (e.g. amorphous, powder or

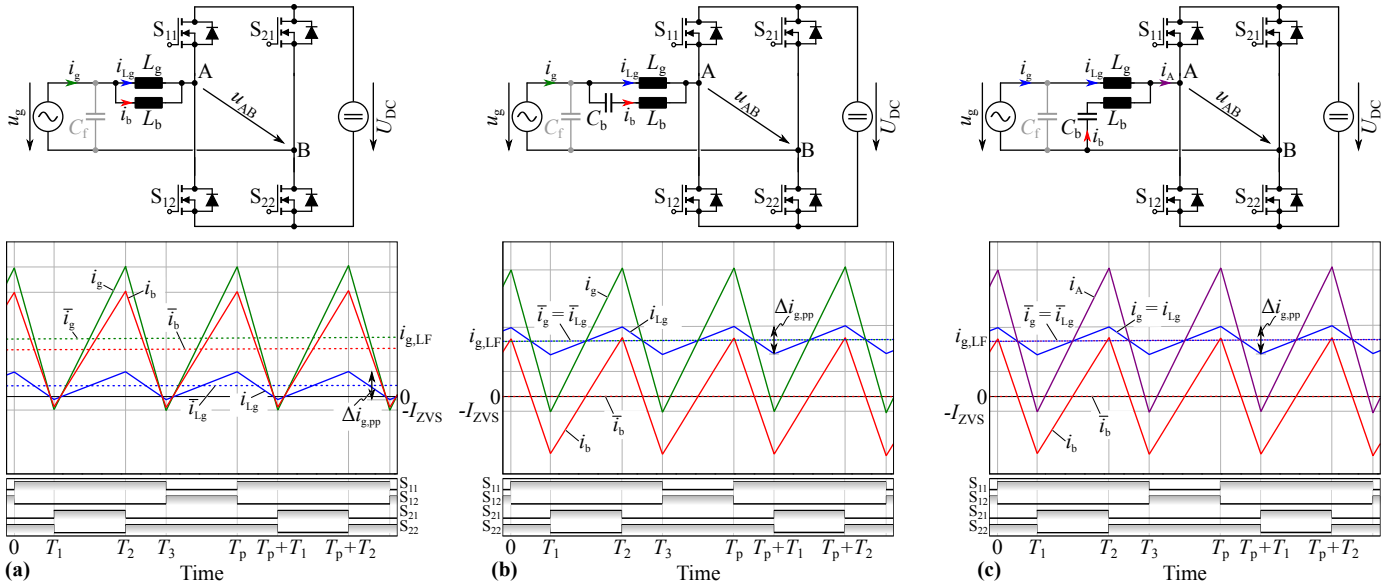


**Fig. 2:** (a) Bidirectional full-bridge AC/DC converter with an additional inductor  $L_b$  in order to increase the current ripple and to obtain soft-switching together with the corresponding current waveforms and their average values (dotted lines). (b) Splitting of the HF and LF currents by adding an LF blocking capacitor  $C_b$  in series to  $L_b$ . The corresponding waveforms show the grid current  $i_g$  as well as the triangular HF current  $i_b$  and the current  $i_{Lg}$  which consists of the total LF current and a small superimposed HF ripple. (c) HF bypassing of the AC-grid by returning the current  $i_b$  via  $C_b$  back into the full-bridge. The grid current  $i_g$  is now again equal to  $i_g$  in the original circuit in Fig. 1 (a). However, soft-switching over the entire grid period is achieved.

nanocrystalline core material) would be needed. Hence, with TCM operation, a reasonable trade-off between HF and LF losses has to be found in the design of the boost inductor. In order to overcome this issue, in this paper the concept of the *integrated* Triangular Current Mode (*iTCM*) operation, known from [9], is introduced. By adding an LC-circuit to the well-known full-bridge-based PWM AC/DC converter, the TCM current can be split into its HF and LF current components, which are now flowing through two separate inductors. Since the superposition of HF and LF current, i.e. the TCM current, is only needed in the semiconductor devices to guarantee soft-switching, this current separation enables a dedicated design of the two inductors, i.e. either optimized for LF or HF currents, and thus results in an expected efficiency improvement. A further advantage of the *iTCM* concept is that the well-known PWM modulation scheme still can be applied and no additional control or measurement circuitry, e.g. current zero crossing detection as needed in TCM operation, is required.

## II. THE INTEGRATED TRIANGULAR CURRENT MODE (*iTCM*) CONCEPT

In practice, for the operation of the conventional PWM full-bridge AC/DC converter (cf. Fig. 1 (a)) the boost inductor  $L_g$  is typically selected relatively large in order to keep the current ripple  $\Delta i_{g,pp}$  small, e.g. within 10%...40% of the peak LF current. In Fig. 1 (b), the grid voltage  $u_g$  and the corresponding inductor current  $i_g$  are shown over an entire mains period. As can be noticed, due to the large inductor value, for the shown time section, the inductor current remains positive during the whole switching cycle, independently of the applied modulation scheme. In the following, the unipolar

PWM modulation scheme with 180° phase-shifted bridge-legs is considered, since in this case the effective switching frequency is doubled, leading to an even smaller current ripple in the boost inductor  $L_g$  (cf. Fig. 1 (c)). Consequently, soft-switching is only achieved in the transitions at the time instants  $t = 0$  (for  $S_{11}$ ) and  $t = T_2$  (for  $S_{22}$ ), whereby hard-switching occurs at the time instants  $t = T_1$  (for  $S_{21}$ ) and  $t = T_3$  (for  $S_{12}$ ). In order to achieve also soft-switching at  $t = T_1$  and  $t = T_3$ , the inductor current would have to change its sign, hence a higher current ripple is required, as it is realized with the Triangular Current Mode (TCM) modulation scheme [5]–[8]. A higher current ripple can e.g. be attained by connecting an inductor with a low inductance value  $L_b$  in parallel to  $L_g$ , as shown in Fig. 2 (a). The grid current  $i_g$ , which is the superposition of the two currents  $i_{Lg}$  and  $i_b$ , is now negative at the time instants  $t = T_1$  and  $t = T_3$ , which means that soft-switching is achieved. Actually, the total current  $i_g$  is equal to the current of a full-bridge converter operated with the TCM modulation scheme. The only difference is that the total TCM current is now split into two currents. Since the same voltage  $u_g - u_{AB}$  is applied to  $L_g$  and  $L_b$ , both inductors exhibit the same shape of their current waveform, whose LF and HF amplitudes only depend on the ratio of  $L_g$  and  $L_b$ . Due to the much smaller inductance of  $L_b$  compared to  $L_g$ , the HF but also the LF current is mainly flowing through  $L_b$  (cf. Fig. 2 (a)). In order to prevent any DC or LF current from flowing through  $L_b$ , a capacitor  $C_b$  can be added in series to  $L_b$ , as shown in Fig. 2 (b). Consequently,  $L_b$  now carries only the HF current and  $L_g$  conducts the total LF current with a small superimposed HF ripple (cf. Fig. 2 (b)). As can be noted, even if  $C_b$  is added, the total grid current remains

unchanged. Instead of connecting the  $L_b/C_b$ -branch directly in parallel to  $L_g$ , it is also possible to connect the  $L_b/C_b$ -branch in parallel to the  $L_g/C_f$ -branch [9], as shown in **Fig. 2 (c)**, where  $C_f$  embodies the typically needed filter capacitor. The two currents  $i_{L_g}$  and  $i_b$  are not affected by this modification, since both LC-branches are now filtering the same voltage  $u_{AB}$ , which means that the LF voltages across  $C_f$  and  $C_b$  have to be the same, i.e. the grid voltage  $u_g$ . Consequently, also the voltages applied to the inductors  $L_g$  and  $L_b$  have to be equal, resulting in the same currents  $i_{L_g}$  and  $i_b$  as obtained in **Fig. 2 (b)**. However, even though the capacitor  $C_b$  now has to be designed to block the full grid voltage  $u_g$ , the advantage of this modification is that the HF current  $i_b$ , which is needed to achieve soft-switching, is no more flowing into the grid, but is kept internally in the circuit. Therefore, this concept is called *integrated* Triangular Current Mode (*iTCM*) concept.

Compared to the initial full-bridge-based PWM AC/DC converter (cf. **Fig. 1 (a)**), the grid current  $i_g$  is not affected by the *iTCM* concept and thus, the EMI filter effort towards the AC grid remains the same. However, due to soft-switching in case of *iTCM* operation, the switching losses are drastically reduced compared to the hard-switched PWM converter. Hence, with the *iTCM* concept, a higher switching frequency can be applied, which means that for the same current ripple in  $L_g$ , a smaller inductance value  $L_g$  can be selected. Even though an LC-branch has to be added for *iTCM* operation, the power density can be increased compared to PWM operation, if the additional volume of the LC-branch is smaller than the saved volume of the typically bulky boost inductor  $L_g$ . Consequently, compared to the conventional PWM converter, a higher efficiency and power density is feasible by employing the *iTCM* concept.

Comparing the *iTCM* concept to TCM operation, the advantages of the *iTCM* concept are not that evident, since the TCM operation does not require a bulky boost inductor  $L_g$  but only a similarly small inductor such as  $L_b$ . Even though with the *iTCM* concept the high current ripple is kept internally, the filtering effort with TCM operation is actually even lower than with *iTCM* operation, since with TCM operation, the two LC branches  $L_g/C_f$  and  $L_b/C_b$  would not be connected in parallel but in series (cf. **Fig. 3 (a)**), resulting in an even better filtered grid current. On the other hand, since in *iTCM* operation the capacitor  $C_b$  does not contribute to the input filter performance, the capacitance  $C_b$  can be selected smaller than the capacitor value needed in a TCM filter structure, thus compensating again for the worse filter attenuation. Nevertheless, the two major advantages of the *iTCM* concept compared to TCM operation seen by the authors are the following:

- 1) In *iTCM* operation, dedicated optimal designs for both inductors  $L_g$  and  $L_b$  are possible. This means that on the one hand,  $L_g$  can be designed for minimum LF losses by selecting a magnetic core material with a high saturation flux density and solid wire windings in order to maximize the copper filling factor. On the other hand,  $L_b$  can be designed for optimum HF properties since there is no DC or LF flux present. Thus, a core material with good HF performance and HF litz wire for low HF conduction

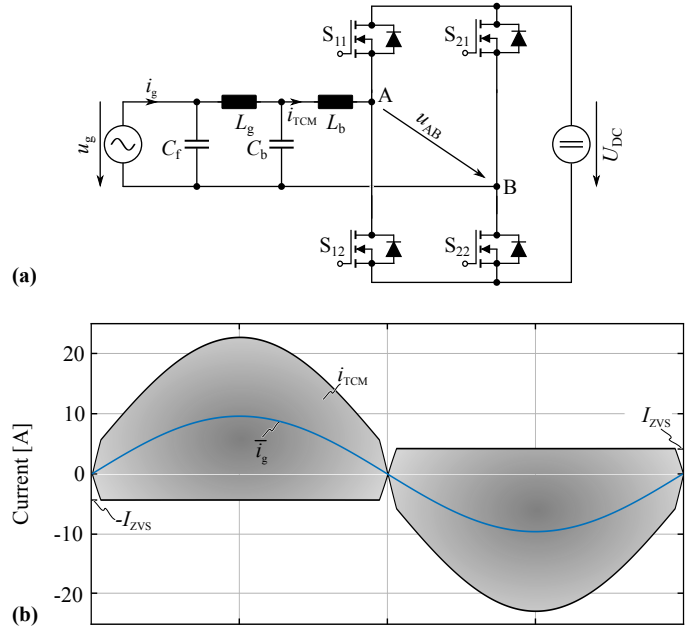


**Fig. 3:** (a) Resulting TCM filter structure if all filtering elements required for *iTCM* operation are used as input filter for a TCM converter. Compared to the parallel filter structure of the *iTCM* concept shown in **Fig. 2 (c)**, the two stage LC filter of the TCM converter leads to a higher HF attenuation towards the AC grid. (b) Envelope of the current  $i_{TCM}$  together with the average grid current  $i_g$  in case of TCM operation of the full-bridge AC/DC converter. Note that the peak current through  $L_b$  is more than twice the average grid current in TCM operation.

losses has to be selected. As already mentioned, in contrast to these two optimized inductors, the inductor design for TCM modulation is more challenging and typically results in a suboptimal inductor design, since it has to conduct the HF and the LF currents at the same time, as can be seen in **Fig. 3 (b)**. Therefore, with the *iTCM* concept an increased efficiency of the inductors as well as of the whole system is expected.

- 2) With the *iTCM* concept, the converter can still be controlled with the simple PWM modulation scheme. Even though TCM modulation is in general not more complex than PWM, the PWM modulation can profit from the fact that most of the commercial DSPs and microcontrollers already incorporate a PWM-unit but not a TCM-unit. Hence, for the gate signaling in case of TCM modulation, an additional real time unit as e.g. an FPGA is required. Furthermore, a current zero-crossing detection is beneficial to properly control the triangular current, which in case of PWM is not needed [8]. Compared to TCM operation, this makes the *iTCM* operation much more robust concerning possible faults and errors in the modulation and the current zero-crossing detection, since with the *iTCM* concept the capacitor  $C_b$  is always blocking any DC-current component such that the current  $i_b$  cannot be subject to a DC drift as e.g. with the TCM modulation. Thus, no additional control besides the grid current control is required for *iTCM* operation.

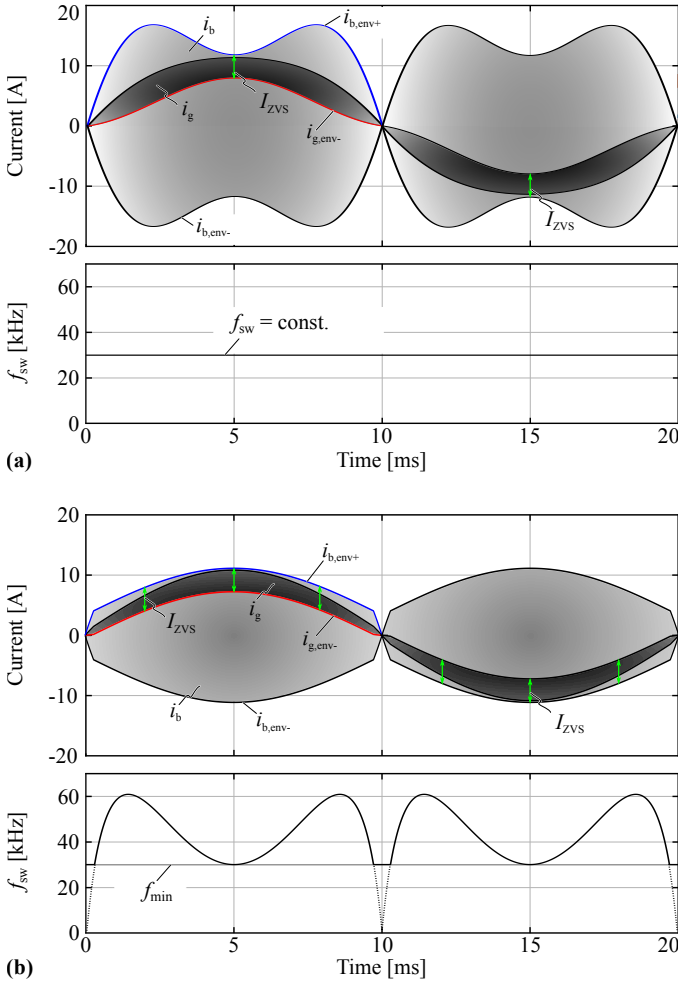


**Fig. 4:** (a) Envelopes of the currents  $i_g$  and  $i_b$  for a constant switching frequency. (b) The switching frequency is adapted in such a way that a constant turn-off current  $I_{ZVS}$  is achieved. For the shown envelopes, the RMS current in the LC-branch is 35% lower in the sine-shaped modulation compared to the constant frequency modulation.

### III. $i$ TCM OPERATION WITH SW. FREQU. MODULATION

Due to the fact that the same HF-voltage is applied to the two inductors  $L_b$  and  $L_g$ , the two current ripples always have the same shape and independently from the AC-voltage always feature the same ratio of their HF current ripple amplitudes, i.e.  $L_g/L_b$ . In **Fig. 4 (a)**, the envelopes of the two current waveforms  $i_g$  and  $i_b$  in the inductors  $L_g$  and  $L_b$  are shown for a constant PWM switching frequency and unity power factor. The upper boundary of the  $i_b$  envelope can be expressed by

$$i_{b,env+} = A(t) \cdot \frac{\hat{u}_g}{2f_{eff}L_b}, \quad \text{whereby} \quad (1)$$

$$A(t) = |\sin(\omega t)| \cdot \left[ 1 - \frac{\hat{u}_g}{U_{DC}} \cdot |\sin(\omega t)| \right], \quad (2)$$

$\omega$  denotes the AC grid angular frequency and  $f_{eff}$  is the effective switching frequency, which is twice the switching frequency of one bridge-leg due to the  $180^\circ$  phase shifted carriers. The same formula holds for the envelope of the HF-ripple in  $L_g$  (except that  $L_b$  has to be replaced by  $L_g$ ). In other words, this means

that the current ripple amplitudes in  $L_g$  and  $L_b$  are always changing proportionally, except that the HF current component of  $i_g$  is superimposed on the LF grid current, whereas the LF current through  $L_b$  is zero. As already mentioned, to achieve soft-switching at the time instants  $t = T_1$  and  $t = T_3$  over the full AC grid period, the instantaneous absolute value of  $i_b$  has to be larger than the instantaneous absolute value of  $i_g$ , i.e.  $|i_b(T_1)| > |i_g(T_1)|$ , or in terms of **Fig. 4**:  $|i_{b,env+}| > |i_{g,env-}|$ . Theoretically assuming that there is no HF current ripple superimposed on  $i_g$  (i.e.  $L_g$  approaches an infinite inductance value), the minimum required amplitude of  $i_b$  is equal to the instantaneous LF AC component in  $L_g$ , i.e.  $i_b(T_1) = i_{g,LF}(T_1)$ . In this case, the switched current of the turning-off MOSFET would be zero ( $I_s = 0$ ). However, in order to be able to fully charge/discharge the parasitic output capacitances  $C_{OSS}$  of the MOSFETs, a certain remaining current  $I_{ZVS}$  is required. Therefore, the current ripple in  $L_b$  has to be increased by  $I_{ZVS}$ , which means  $|i_b(T_1)| \geq |i_{g,LF}(T_1) + I_{ZVS}|$  (cf. **Fig. 2**) or  $|i_{b,env+}| \geq |i_{g,env-} + I_{ZVS}|$  (cf. **Fig. 4**). The minimum required value of  $I_{ZVS}$  can be calculated based on the effective output charge  $Q_{OSS}$  of the switching devices to charge/discharge the output capacitances  $C_{OSS}$  and the maximum allowed duration of this resonant switching transition (i.e. the dead time duration  $T_{dt}$ ) which also defines the minimum and maximum duty cycles of the converter [8]. Hence, in order not to limit the duty cycle range and therewith to be able to control the input/output voltage in a wide range,  $T_{dt}$  has to be small (e.g.  $k = 1\%$ ) compared to the switching period  $T_p$ . The minimum required current  $I_{ZVS}$  can roughly be calculated as

$$I_{ZVS} = Q_{OSS}/T_{dt} = Q_{OSS}/(k \cdot T_p). \quad (3)$$

Due to the limited boost inductance  $L_g$ , in reality, a certain HF current ripple  $\Delta i_{g,pp}$  is inevitable and even beneficial, since for the same switched current  $I_{ZVS}$ , the amplitude of  $i_b$  can be reduced by  $\Delta i_{g,pp}/2$ , which means that the inductance value of  $L_b$  has to be increased. As a consequence, there is a certain degree of freedom in the selection of the inductance ratio  $L_g/L_b$ .

As can be noted in **Fig. 4 (a)**, the switched current (i.e. the difference of  $i_{b,env+}$  and  $i_{g,env-}$ ) is not constant and, due to the PWM modulation, in a wide range much larger than the required value  $I_{ZVS}$ , which unfortunately results in a high RMS current in the inductor  $L_b$  and the switches, thus causing higher conduction losses. In order to avoid these extra losses, in the intervals where  $|i_{b,env+} - i_{g,env-}| > I_{ZVS}$ , the switching frequency can be increased in such a way that both HF current ripples are reduced and in every switching transient the desired current  $I_{ZVS}$  is achieved, i.e.  $|i_{b,env+} - i_{g,env-}| \stackrel{!}{=} I_{ZVS}$ . By solving this equation, where

$$|i_{g,env-}| = \frac{2P}{\hat{u}_g} |\sin(\omega \cdot t)| - A(t) \cdot \frac{\hat{u}_g}{2f_{eff}L_g} \quad (4)$$

and  $P$  equals the converter output power, the required effective

switching frequency can be found as

$$f_{\text{eff}} = \frac{A(t) \hat{u}_g^2}{4P |\sin(\omega \cdot t)| + 2\hat{u}_g I_{ZVS}} \cdot \left( \frac{1}{L_g} + \frac{1}{L_b} \right). \quad (5)$$

The corresponding switching frequency  $f_{\text{sw}} = f_{\text{eff}}/2$  (due to the 180° phase-shifted bridge-legs) together with the resulting envelopes of  $i_g$  and  $i_b$  are shown in **Fig. 4 (b)** for unity power factor operation. As expected, the difference of the two envelopes  $i_{b,\text{env}+}$  and  $i_{g,\text{env}-}$  is now constant over the entire grid period, except in vicinity of the AC voltage zero crossing, where the switching frequency is limited to a minimum value  $f_{\text{min}}$  above the audible frequency range. Compared to the modulation with constant switching frequency (cf. **Fig. 4 (a)**), the RMS current in the  $L_b/C_b$ -branch can be reduced by 35%, leading to a significant reduction of the conduction losses in both, the switches and the inductor  $L_b$ . Even though the maximum switching frequency is now approximately twice as high as in case of the constant frequency modulation, the change in switching losses finally depends on the MOSFET's soft-switching characteristics, since on the one hand a lower current is switched, but at a higher frequency. However, in soft-switched topologies, the conduction losses are typically dominating over the switching losses, resulting in lower total losses, as also shown in Section V.

#### IV. DESIGN CRITERIA AND DIMENSIONING OF THE LC-BRANCH

For the design of the LC-branch, the system power  $P$ , the peak AC grid voltage  $\hat{u}_g$ , the minimum ZVS current  $I_{ZVS}$  and the maximum relative peak-to-peak grid current ripple  $r = \Delta i_{g,\text{pp}}/\hat{i}_g$  (e.g.  $r = 40\%$  of the peak grid current) have to be known. Initially, the grid inductance  $L_g$  required to comply with the maximum allowed current ripple  $r$  can be calculated by

$$L_g = \frac{\hat{u}_g^2}{2r f_{\text{eff},\text{min}} P} \left( 1 - \frac{\hat{u}_g}{U_{\text{DC}}} \right). \quad (6)$$

In order to determine the inductance value  $L_b$ , (6) is inserted into (5) and solved for  $L_b$ . In addition,  $\sin(\omega t)$  is set to one, since in case of a switching frequency variation, the maximum current ripple occurs at the peak of the grid voltage, where also the effective switching frequency reaches its minimum (cf.  $f_{\text{sw}}$  in **Fig. 4 (b)**). Hence,  $L_b$  can be calculated as

$$L_b = \frac{\hat{u}_g^2}{2P(2-r) + 2I_{ZVS}\hat{u}_g} \left( 1 - \frac{\hat{u}_g}{U_{\text{DC}}} \right) \frac{1}{f_{\text{eff},\text{min}}}. \quad (7)$$

Furthermore, as already mentioned, capacitor  $C_b$  is needed to block any LF or DC current flowing through the LC-branch. Since for low frequencies,  $C_b$  is connected in parallel to the grid (the impedance of  $L_g$  and  $L_b$  (cf. **Fig. 2 (c)**) is negligible at the mains frequency),  $C_b$  leads to an additional reactive power consumption from the AC grid. For this reason, and in order to minimize the volume of  $C_b$ , the capacitance value should be small. On the other hand, in order to achieve soft-switching, a certain minimum inductive current through the LC-branch is required. Consequently, the capacitance of  $C_b$  has to be selected sufficiently large such that the LC-resonance

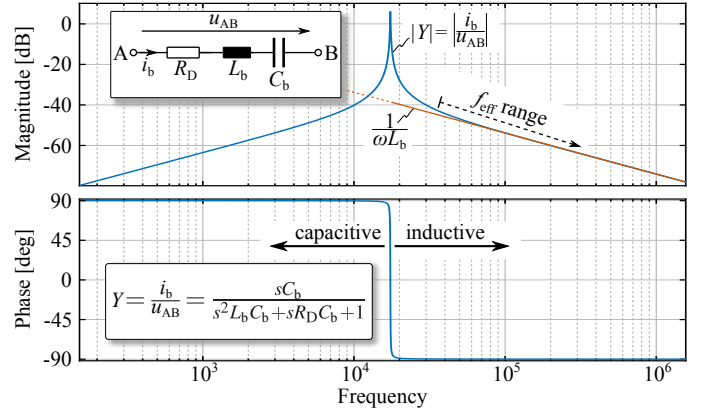


**Fig. 5:** Bode diagram of the transfer function of the LC-circuit.  $R_D$  models the series resistance of the inductor. The LC-circuit has to be designed such that the effective switching frequency range is well above the resonance.

frequency is well below the effective switching frequency range  $f_{\text{eff}}$ . **Fig. 5** shows the bode diagram of the LCR transfer function

$$Y = \frac{i_b}{u_{AB}} = \frac{sC_b}{s^2 L_b C_b + s R_D C_b + 1}, \quad (8)$$

and the reasonable range of the effective switching frequency  $f_{\text{eff}}$ . It can be seen that a selection of the resonance frequency too close to the minimum effective switching frequency would lead to a deviation from a purely inductive behaviour, indicated as  $1/\omega L_b$  in **Fig. 5**, which would result in a strong increase of the current amplitude (for only small changes in the switching frequency ( $|Z| = \omega L_b - 1/\omega C_b$ , if  $R_D$  is neglected)). Therefore, the influence of the capacitor  $C_b$  on the current amplitude should be kept small such that  $I_{ZVS}$  is not changed by more than e.g.  $d = 10\%$ . This translates into the condition that the relative change in the impedance  $|Z|$  caused by  $C_b$  should be smaller than  $d \cdot \frac{I_{ZVS}}{\hat{i}_b}$  at the lowest effective switching frequency  $f_{\text{eff},\text{min}}$ , i.e.

$$\frac{\omega_{\text{eff},\text{min}} L_b - \left( \omega_{\text{eff},\text{min}} L_b - \frac{1}{\omega_{\text{eff},\text{min}} C_b} \right)}{\omega_{\text{eff},\text{min}} L_b} \leq d \cdot \frac{I_{ZVS}}{\hat{i}_b}, \quad (9)$$

whereby  $\hat{i}_b = \frac{\hat{u}_g}{2f_{\text{eff},\text{min}} L_b} \left( 1 - \frac{\hat{u}_g}{U_{\text{DC}}} \right)$  is obtained from (1) with  $\sin(\omega t) = 1$ . The value  $C_b$  can now be determined by solving (9) for  $C_b$

$$C_b \geq \frac{\hat{i}_b}{4\pi^2 f_{\text{eff},\text{min}}^2 L_b I_{ZVS} \cdot d}, \quad (10)$$

and defines the lower limit for the capacitance  $C_b$ .

#### V. DESIGN OF THE MEDIUM-VOLTAGE GRID CONNECTED AC/DC CONVERTER

Although there are no mandatory requirements regarding conducted EMI for medium voltage (MV) grid applications, it is reasonable to limit the EMI emission into the MV grid by means of filtering. Therefore, the PWM approach (cf. **Fig. 1 (a)**) in combination with a small current ripple (i.e. high value of  $L_g$ ) would be a reasonable topology for a MV-connected AC/DC converter. However, the prominent hard-switching losses of high blocking voltage SiC devices either strongly deteriorate

**TABLE I:** Comparison between the inductive components for PWM, TCM and *i*TCM operation.

Mode	$\bar{f}_{\text{eff}}$ [kHz]	$L_g$ [mH]	$L_b$ [ $\mu\text{H}$ ]	$\hat{I}_{Lb}$ [A]	$I_{Lb,\text{rms}}$ [A]	$\hat{E}_{\text{mag},Lb}$ [mJ]	$\hat{I}_{Lg}$ [A]	$\hat{E}_{\text{mag},Lg}$ [mJ]
PWM, 10 kHz	20	23.6	-	-	-	-	10.9	1402
<i>i</i> TCM, $f_{\text{sw}} = \text{const}$	60	7.9	905	16.1	8.2	117.3	10.9	469
<i>i</i> TCM, sine-shaped	91.6	5.6	905	11.4	5.3	58.8	11.1	345
Normal TCM	91.6	5.6	778	22.6	8.9	198.7	11.1	345

the achievable efficiency or lead to a poor power density, since the switching frequency has to be selected rather low. Therefore, the proposed *i*TCM concept is a very attractive solution in MV AC/DC applications. For this reason, the *i*TCM concept is applied to a 10 kV SiC-MOSFET-based bidirectional single-phase 25 kW AC/DC converter operated from the 6.6 kV<sub>rms</sub> (phase to phase) MV grid as rectifier/inverter stage in a MV AC to 400 V DC Solid-State Transformer [10].

In order to assess the performance of the *i*TCM approach, the conduction and the switching losses of the semiconductors as well as the properties of the inductive components are compared for the different approaches in the following.

For the calculation of the total semiconductor losses, the switching losses of the 10 kV SiC-MOSFETs at hand (Wolf-speed, CPM3-10000-0350) have to be determined. Hence, besides the already published soft-switching losses (cf. **Fig. 6 (a)** and [11]), also hard-switching loss measurements have been performed (cf. **Fig. 6 (b) & (c)**).

In [12], the upper switching frequency limit for these 10 kV SiC devices in hard-switching operation is stated to be 10 kHz. Therefore, this switching frequency is used for the loss calculation of the standard PWM approach. As can be noted from **Fig. 6**, the soft-switching losses of these 10 kV SiC MOSFETs are much lower than the hard-switching losses. Hence, the switching frequency range for the soft-switched TCM and *i*TCM designs can be increased and is set to  $[f_{\text{min}}, f_{\text{max}}] = [30 \text{ kHz}, 65 \text{ kHz}]$  in order to not only increase the efficiency, but also the power density compared to the hard-switched PWM modulation. In case of PWM and *i*TCM operation, the maximum peak-to-peak grid current ripple  $\Delta i_{g,\text{pp}}$  is set to  $r = 40\%$  of the peak grid current. For PWM operation, the resulting boost inductance is

$$L_{g,\text{PWM}} = \frac{U_{\text{DC}} \hat{u}_g}{8r f_{\text{eff}} P} = 23.6 \text{ mH} \quad (11)$$

(for a duty cycle of 50% and  $f_{\text{eff}} = 2 \cdot 10 \text{ kHz} = 20 \text{ kHz}$ ) and for *i*TCM modulation it is only

$$L_{g,i\text{TCM}} = 5.6 \text{ mH} \quad (12)$$

(calculated via (6) for  $f_{\text{eff}} = 2 \cdot 30 \text{ kHz} = 60 \text{ kHz}$ ). Furthermore, with a ZVS current of  $I_{\text{ZVS}} = 4 \text{ A}$ , a maximum deviation of  $I_{\text{ZVS}}$  by  $d = 10\%$  due to the insertion of  $C_b$  and a minimum switching frequency of  $f_{\text{min}} = 30 \text{ kHz}$  (i.e.  $f_{\text{eff},\text{min}} = 2 \cdot 30 \text{ kHz} = 60 \text{ kHz}$ ), the component values of the LC-branch  $L_b = 905 \mu\text{H}$  and  $C_b = 221.9 \text{ nF}$  are obtained from (7) and (10), respectively. In this case, the reactive power flow caused

by  $C_b$  is approximately 1 kvar, leading to a power factor of  $\lambda > 0.999$ . Hence,  $C_b$  hardly influences the power factor.

In case of conventional TCM modulation, the corresponding TCM inductance value can also be obtained from (7) by inserting  $r = 0$ , since in this case the entire current ripple is carried by the TCM inductor. Accordingly, the required inductance value for conventional TCM modulation is  $L_b = 778 \mu\text{H}$ , which is slightly smaller than the inductance value  $L_b$  needed for *i*TCM operation.

However, comparing the magnetic components of the different concepts, it can be seen from **TABLE I** that the inductance value of the bulky boost inductor  $L_g$  in case of PWM operation can be reduced by more than a factor of four with the *i*TCM concept without changing the current ripple  $\Delta i_{g,\text{pp}}$ , since with *i*TCM operation, a higher switching frequency can be applied. This also translates into a four times lower magnetic energy stored in  $L_g$  and therefore, approximately a four times smaller inductor volume can be expected.

For the comparison of the filter size, it is assumed that for both, TCM and *i*TCM operation, approximately the same filter inductance value  $L_g$  is required (cf. **Fig. 3 (a)**), leading to the same volume of  $L_g$  in both cases. On the other hand, comparing the HF inductors  $L_b$  of the TCM and the *i*TCM concept, it is evident from **TABLE I** that for the same switching frequency, the TCM inductance value is slightly smaller than the *i*TCM inductance value. However, since the TCM inductor also has to conduct the LF current, its peak current is much higher than for *i*TCM operation which in this case leads to a three times higher peak magnetic energy and therefore also a three times larger volume is expected. Furthermore, it can be expected that compared to TCM modulation, with the *i*TCM concept a higher efficiency can be achieved, since both inductors  $L_g$  and  $L_b$  can be optimized separately, whereas for the TCM inductor, a compromise between good LF and HF properties has to be found.

Based on the given design parameters, the RMS currents in the switches and the LC-branch, as well as the average switched currents within an entire grid period are obtained by circuit simulation for all three modulation concepts as listed in **TABLE II**. The conduction losses  $P_c$  can now be calculated for the four switches as  $P_c = 4R_{\text{DS,on}} I_{\text{FET,rms}}^2$ , whereas the on-state resistance is assumed to be  $R_{\text{DS,on}} = 750 \text{ m}\Omega$  for a junction temperature of 100 °C. Furthermore, due to the almost linear behaviour of the switching energies with respect to the switched current (cf. **Fig. 6**), the switching losses can

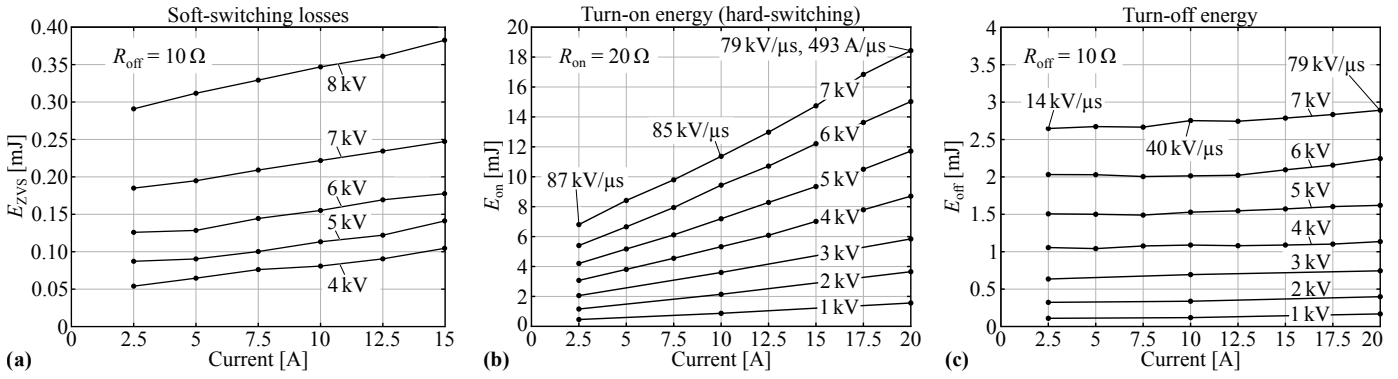


**Fig. 6:** (a) Calorimetrically measured soft-switching losses with an external turn-off gate resistor of  $10\ \Omega$ , cf. Fig. 8 in [11]. (b) Measured turn-on and (c) turn-off energies of the  $10\ \text{kV}$  SiC MOSFETs operated at  $25\ ^\circ\text{C}$  with an external turn-on gate resistor of  $20\ \Omega$  and turn-off gate resistor of  $10\ \Omega$ .

**TABLE II:** Comparison between PWM, TCM and the different *i*TCM modulation schemes, whereby  $I_{ZVS} = 4\ \text{A}$  is chosen. For PWM, the designation for  $\bar{I}_{sw}$  is  $\bar{I}_{sw,on}$  (hard) /  $\bar{I}_{sw,off}$  (soft). For the other modulation concepts, the designation for  $\bar{I}_{sw}$  is  $\bar{I}_{sw,off}$  (soft).

Mode	$I_{FET,rms}$ [A]	$I_{TCM,rms}$ [A]	$\bar{I}_{sw}$ [A]	$\bar{E}_{sw}$ [mJ]	$\bar{f}_{sw}$ [kHz]	$P_c$ [W]	$P_{sw}$ [W]	$P_{tot}$ [W]
PWM, 10 kHz	4.7	-	4.5 / 7.4	10.8	10	66.3	216	282.3
<i>i</i> TCM, $f_{sw} = \text{const}$	8.1	8.2	15.0	0.247	30	196.8	29.6	226.4
<i>i</i> TCM, sine-shaped	6.3	5.3	9.4	0.219	45.8	119.1	40.1	159.2
Normal TCM	6.3	-	9.4	0.219	45.8	119.1	40.1	159.2

be calculated based on the average switched currents and the average switching frequencies. Considering **TABLE II**, with the sine-shaped *i*TCM concept, the conduction losses are increasing by  $52.8\ \text{W}$  compared to PWM operation, however, the switching losses can be reduced by  $175.9\ \text{W}$  which means that the total semiconductor losses are decreased by  $123.1\ \text{W}$  or  $43.6\ \%$ . Furthermore, comparing the TCM and the *i*TCM concepts, it can be seen that there is no difference in the semiconductor losses, since with both modulations exactly the same current waveforms can be generated.

## VI. CONCLUSION

In this paper, the *integrated* Triangular Current Mode (*i*TCM) concept, which is a simple method to achieve soft-switching over the entire AC grid period in a bidirectional AC/DC converter, is presented. Compared to the conventional hard-switched PWM modulation scheme, for the given example of a  $10\ \text{kV}$  SiC-MOSFET-based bidirectional  $25\ \text{kW}$  single-phase AC/DC converter, with the *i*TCM concept the average switching frequency can be increased by a factor of almost five, whereas at the same time the semiconductor losses could be even reduced by more than  $40\ \%$ . Furthermore, due to the higher switching frequency, the inductance value of the bulky boost inductor  $L_g$  can be reduced by more than a factor of four without changing the current ripple  $\Delta i_{g,pp}$  injected into the MV grid, which means that the *i*TCM concept allows to push the Pareto front towards higher power densities and efficiencies simultaneously. Even compared to the conventional TCM modulation, an improvement concerning power density and efficiency can be expected, since with the *i*TCM modulation,

the total stored magnetic energy in the system is reduced and the two inductors can be separately optimized for HF and LF currents. Furthermore, with the *i*TCM concept, still the well-known PWM modulation scheme (optionally with variable switching frequency) can be applied and no additional current zero crossing detection, as needed for TCM operation, is required.

## ACKNOWLEDGEMENT

This research project is part of the National Research Programme Energy Turnaround (NRP 70) of the Swiss National Science Foundation (SNSF). Further information on the National Research Programme can be found at [www.nrp70.ch](http://www.nrp70.ch).

## REFERENCES

- [1] J. Thoma, D. Chilachava, and D. Kranzer, "A Highly Efficient DC-DC Converter for Medium-Voltage Applications," in *Proc. IEEE Int. Energy Conf. (ENERGYCON)*, Dubrovnik, Croatia, 2014, pp. 140–144.
- [2] K. Vechalapu, S. Bhattacharya, E. V. Brunt, S.-h. Ryu, and D. Grider, "Comparative Evaluation of  $15\ \text{kV}$  SiC MOSFET and  $15\ \text{kV}$  SiC IGBT for Medium Voltage Converter under Same  $dv/dt$  Conditions," in *Proc. IEEE Energy Conversion Congr. and Expo. (ECCE)*, Montreal, Canada, 2015, pp. 927–934.
- [3] J. Thoma and D. Kranzer, "Demonstration of a Medium Voltage Converter with High Voltage SiC Devices and Future Fields of Application," in *Proc. Conf. on Power Conversion and Intelligent Motion (PCIM)*, Nuremberg, 2015, pp. 111–118.
- [4] K. Vechalapu and S. Bhattacharya, "Performance Comparison of  $10\ \text{kV}$ - $15\ \text{kV}$  High Voltage SiC Modules and High Voltage Switch using Series Connected  $1.7\ \text{kV}$  LV SiC MOSFET devices," in *Proc. IEEE Energy Conversion Congr. and Expo. (ECCE)*, Milwaukee, USA, 2016.
- [5] C. Henze, H. Martin, and D. Parsley, "Zero-Voltage Switching in High Frequency Power Converters using Pulse Width Modulation," in *Proc. IEEE Appl. Power Electron. Conf. and Expo. (APEC)*, 1988, pp. 33–40.

- [6] C. Marxgut, J. Biela, and J. W. Kolar, "Interleaved Triangular Current Mode ( TCM ) Resonant Transition , Single Phase PFC Rectifier with High Efficiency and High Power Density," in *Proc. IEEE Int. Power Electron. Conf. (IPEC)*, Sapporo, Japan, 2010, pp. 1725–1732.
- [7] C. Marxgut, F. Krismer, D. Bortis, and J. W. Kolar, "Ultraflat Interleaved Triangular Current Mode (TCM) Single-Phase PFC Rectifier," *IEEE Trans. Power Electron.*, vol. 29, no. 2, pp. 873–882, 2014.
- [8] D. Bortis, D. Neumayr, and J. W. Kolar, " $\eta\rho$  -Pareto Optimization and Comparative Evaluation of Inverter Concepts considered for the GOOGLE Little Box Challenge," in *Proc. IEEE Workshop on Control and Model. of Power Electron. (COMPEL)*, Trondheim, 2016.
- [9] M. Pahlevaninezhad, S. Pan, and P. Jain, "ZVS Voltage Source Inverter," *U.S. Patent Application 2015/0194909 A1*, 2015.
- [10] D. Rothmund, G. Ortiz, T. Guillod, and J. W. Kolar, "10kV SiC-Based Isolated DC-DC Converter for Medium Voltage-Connected Solid-State Transformers," in *Proc. IEEE Appl. Power Electronics Conf. (APEC)*, Charlotte, USA, 2015.
- [11] D. Rothmund, D. Bortis, and J. W. Kolar, "Accurate Transient Calorimetric Measurement of Soft-Switching Losses of 10kV SiC MOSFETs," in *Proc. Int. Symposium on Power Electron. for Distributed Generation Systems (PEDG)*, Vancouver, 2016.
- [12] J. B. Casady, E. V. Brunt, G.-y. Wang, J. Richmond, S. T. Allen, and D. Grider, "New Generation 10kV SiC Power MOSFET and Diodes for Industrial Applications," in *Proc. Conf. on Power Conversion and Intelligent Motion (PCIM)*, Nuremberg, 2015, pp. 96–103.